

The Interference Effect of Top Quark Polarization at Hadronic Colliders

Darwin Chang^(1,2), Shih-Chang Lee⁽²⁾ and Paul Turcotte⁽¹⁾

⁽¹⁾*Physics Department, National Tsing-Hua University, Hsinchu 30043, Taiwan, R.O.C.*

⁽²⁾*Institute of Physics, Academia Sinica, Taipei, R.O.C.*

Abstract

We derive a simple analytic expression for $q\bar{q}, gg \rightarrow t\bar{t} \rightarrow bW^+\bar{b}W^- \rightarrow b\bar{l}\nu_l\bar{b}l'\bar{\nu}_{l'}$ for on shell intermediate states with the interference effects due to the polarizations of the t and \bar{t} . We then investigate how this effect may be measured at Tevatron or other hadronic colliders.

arXiv:hep-ph/9508357v1 23 Aug 1995

The experimental groups at Tevatron has already provided strong evidence for the top quark with mass around 174 GeV [1]. In the near future, the data related to the production of the top quark is going to accumulate very quickly. Top quark decays very rapidly after its production. Therefore, it is challenging to investigate how one can determine the various detail properties of top quark in the complex hadronic collider environment.

In this paper, we investigate an interesting physical consequence of the fact that the top quarks that are produced and decayed are supposed to be spin 1/2 particles. Due to the confinement phenomena of the strong interaction, the spin of a quark is in general very difficult to measure directly. Even if the quark is produced in a particular polarized state, the spin information is quickly averaged out by the hadronization process. One of the important effect of the polarizations of unstable particles are that the different polarized intermediate states can interfere. For lighter quarks, this effect may be smeared heavily by the hadronization process. However, in the case of the top quark, because of its mass, the decay rate is much faster than for the other quarks. The top quark decays before the hadronization effect has the time to smear its polarization information at production [2]. This allows us to neglect the effect of hadronization. The same can not be said of any other quarks. Therefore, in this sense, this polarization effect also provide a unique possibility of direct observation of the spin of a quark.

We use an analytic helicity technique developed in ref. [4] to calculate the cross section $q\bar{q}$ and $gg \rightarrow t\bar{t} \rightarrow bW^+\bar{b}W^- \rightarrow b\bar{\nu}_i\bar{b}'\nu_i$. This cross section includes 6 particles in the final state. We derive simple analytic expressions including the interference effect, and then give the exact differential cross section assuming that the top quarks and the W bosons are on-shell. The decays of W bosons and top quarks are taken into account in the narrow width approximation. It is clear that the contribution due to the off-shell top quarks or the off-shell W bosons are negligible. The interference effects discussed here was also considered before in ref. [7], however, it was studied only numerically and was done in a rougher approximation. The analytic expressions obtained here also allows us to make simple analysis about how such effect may be observable at Tevatron and future colliders.

To calculate the cross section using an analytic helicity technique, we split the process into many subprocesses that can be calculated independently. In our case, the polarization density matrix is split into two main sections and can be written as

$$P = \frac{1}{N_s} \sum_{\lambda_1, \lambda_2, \lambda_3, \lambda_3', \lambda_4, \lambda_4'} P(i_{\lambda_1 \lambda_1} \bar{i}_{\lambda_2 \lambda_2} \rightarrow t_{\lambda_3 \lambda_3'} \bar{t}_{\lambda_4 \lambda_4'}) |\Pi_t(r_1)|^2 |\Pi_{\bar{t}}(r_2)|^2 \times P(t_{\lambda_3 \lambda_3'} \bar{t}_{\lambda_4 \lambda_4'} \rightarrow b\bar{b}l^+l^-\nu\bar{\nu}). \quad (1)$$

Here the initial the final polarizations are summed over. N_s is the number of initial states to be averaged over. $N_s = 4(N^2 - 1)^2$ for gg initial states; and $N_s = 4N^2$ for $q\bar{q}$ initial states. $\Pi_q(r_i) = -i(r_i^2 - m_q^2)^{-1}$ is the propagator for a scalar particle. Here, $\Pi_t(r_1)$ and $\Pi_{\bar{t}}(r_2)$ represent the polarization independent components of the top quark propagators with the four-momenta r_1 and r_2 respectively. The helicity informations are included in the remaining density matrices. The polarization density matrix P is defined by

$$P(a_{ij} \dots \rightarrow b_{kl} \dots) = M(a_i \dots \rightarrow b_k \dots) M^\dagger(a_j \dots \rightarrow b_l \dots) \quad (2)$$

with M being the amplitude for the process. When no subscript is included for a given particle with spin in P , it implies that its helicity is summed over. The polarization density matrix $P(i_{\lambda_1 \lambda_1} \bar{i}_{\lambda_2 \lambda_2} \rightarrow t_{\lambda_3 \lambda_3'} \bar{t}_{\lambda_4 \lambda_4'})$ represents the production of the top quark pair via the processes $q\bar{q} \rightarrow t\bar{t}$ or $gg \rightarrow t\bar{t}$. They have been calculated analytically in detail in ref. [4]. $P(t_{\lambda_3 \lambda_3'} \bar{t}_{\lambda_4 \lambda_4'} \rightarrow b\bar{b}ll\nu\nu)$ is the polarization density matrix for the decay of the top quark pair into b quarks and leptons. This density matrix can be further splitted into the product of the decay density matrix of $t\bar{t}$ into W^+W^- bosons and $b\bar{b}$ pairs, and the decay density matrix of W^+W^- boson pair into a pair of fermions each. The main advantage of this technique is that helicity density matrix of each subprocess can be calculated separately independent of each other. The results can then be applied to the calculation of different processes by gluing the density matrix of the subprocesses together.

Therefore the polarized density matrix of the process $t_{\lambda_3 \lambda_3'} \bar{t}_{\lambda_4 \lambda_4'} \rightarrow b\bar{b}ll\nu\nu$ can be written as

$$\begin{aligned}
P(t_{\lambda_3\lambda'_3}\bar{t}_{\lambda_4\lambda'_4} \rightarrow b\bar{b}l^+\nu\bar{\nu}) &= \sum_{\lambda_5,\lambda'_5,\lambda_6,\lambda'_6} P(t_{\lambda_3\lambda'_3} \rightarrow W_{\lambda_5\lambda'_5}^+ b) P(\bar{t}_{\lambda_4\lambda'_4} \rightarrow W_{\lambda_6\lambda'_6}^- \bar{b}) |\Pi_W(p_1)|^2 \\
&\times |\Pi_W(p_2)|^2 P(W_{\lambda_5\lambda'_5}^+ \rightarrow l^+\bar{\nu}) P(W_{\lambda_6\lambda'_6}^- \rightarrow l^-\nu) \quad (3)
\end{aligned}$$

which can be explicitly calculated to be

$$\begin{aligned}
P(t_{\lambda_3\lambda'_3} \rightarrow W_{\lambda_5\lambda'_5}^+ b) &= m_t \left(\frac{e^2 |V_{tb}|^2}{2 \sin^2 \theta_w} \right) [q_1^\mu g^{\nu\rho} - g^{\mu\nu} q_1^\rho + q_1^\nu g^{\mu\rho} - i\epsilon^{\sigma\mu\nu\rho} q_{1\sigma}] \\
&\times \epsilon_{1\mu}^*(\lambda_5) \epsilon_{1\nu}(\lambda'_5) e_\rho^a(r_1) \sigma_{a(\lambda_3\lambda'_3)}, \quad (4)
\end{aligned}$$

$$\begin{aligned}
P(\bar{t}_{\lambda_4\lambda'_4} \rightarrow W_{\lambda_6\lambda'_6}^- \bar{b}) &= m_t \left(\frac{e^2 |V_{tb}|^2}{2 \sin^2 \theta_w} \right) [q_2^\mu g^{\nu\rho} - g^{\mu\nu} q_2^\rho + q_2^\nu g^{\mu\rho} + i\epsilon^{\sigma\mu\nu\rho} q_{2\sigma}] \\
&\times \epsilon_{2\mu}^*(\lambda_6) \epsilon_{2\nu}(\lambda'_6) e_\rho^a(r_2) \bar{\sigma}_{a(\lambda_4\lambda'_4)}, \quad (5)
\end{aligned}$$

$$P(W_{\lambda_5\lambda'_5}^+ \rightarrow l^+\nu) = \left(\frac{e^2}{\sin^2 \theta_w} \right) [k_1^\mu l_1^\nu + k_1^\nu l_1^\mu - g^{\mu\nu} k_1 \cdot l_1 + i\epsilon^{\sigma\mu\rho\nu} k_{1\sigma} l_{1\rho}] \epsilon_{1\mu}(\lambda_5) \epsilon_{1\nu}^*(\lambda'_5) \quad (6)$$

and

$$P(W_{\lambda_6\lambda'_6}^- \rightarrow l^-\bar{\nu}) = \left(\frac{e^2}{\sin^2 \theta_w} \right) [k_2^\mu l_2^\nu + k_2^\nu l_2^\mu - g^{\mu\nu} k_2 \cdot l_2 - i\epsilon^{\sigma\mu\rho\nu} k_{2\sigma} l_{2\rho}] \epsilon_{2\mu}(\lambda_6) \epsilon_{2\nu}^*(\lambda'_6). \quad (7)$$

These results include summations over the helicities of the final state fermions. The four vectors k_i , l_i and q_i correspond to the momenta of the neutrinos, the charged leptons and the b quarks respectively. The subscript 1 is used to label the momenta related to the decay products of the top quark, while the subscript 2 is used for those related to the decay of the anti-top quark. $\epsilon_{1\mu}(\lambda_5)$ represents the polarization vectors of W^+ with helicity λ_5 , while $\epsilon_{2\nu}(\lambda_6)$ represents those of the W^- with helicity λ_6 . In our notation, the information about the top helicity is carried by the Pauli matrix σ_i and $\sigma_0(=1)$ with component $(\lambda_3\lambda'_3)$. For the anti-top, we used the conjugate matrix $\bar{\sigma}_a = \sigma_2 \sigma_a \sigma_2$ with component $(\lambda_4\lambda'_4)$.

The tensor $e^a(r_i)$, ($a = 0, 1, 2, 3$), were introduced in ref. [4] to evaluate the product of fermion wave functions, $u(r, \lambda)\bar{u}(r, \lambda')$, in the amplitude squared for the cross section. They are defined as

$$u(r, \lambda)\bar{u}(r, \lambda') = \frac{1}{2}(m + \not{p}) \left(\not{\epsilon}^0(r) \sigma_{0(\lambda\lambda')} + \not{\epsilon}^i(r) \gamma_5 \sigma_{i(\lambda\lambda')} \right), \quad (8)$$

$$v(r, \lambda)\bar{v}(r, \lambda') = \frac{1}{2}(m - \not{p}) \left(\not{\epsilon}^0(r)\bar{\sigma}_{0(\lambda\lambda')} + \not{\epsilon}^i(r)\gamma_5\bar{\sigma}_{i(\lambda\lambda')} \right). \quad (9)$$

The explicit form of the tensor $e^a(r_i)$ can be found in the reference [4,6], but in our case, we only need the following properties,

$$\sum_{\mu} r^{\mu} e_{\mu}^a(r) = m_t \delta^{0a}, \quad (10)$$

$$\sum_{\mu} e^{a\mu}(r) e_{\mu}^b(r) = g^{ab}, \quad (11)$$

$$\sum_{k=1}^3 e_{\mu}^k(r) e_{\nu}^k(r) = -g_{\mu\nu} + r_{\mu} r_{\nu} / m_t^2. \quad (12)$$

where r is the 4-momentum of either the top quark or the anti-top quark. The spatial component, $e_{\mu}^i(p)$ (i.e. $i = 1, 2, 3$), were first introduced by Bouchiat and Michel [8].

One can then combine the above results for all the subprocesses and use the narrow width approximation for the W boson propagators to obtain

$$\begin{aligned} P(t_{\lambda_3\lambda'_3} \bar{t}_{\lambda_4\lambda'_4} \rightarrow b\bar{b}ll\nu\nu) &= 16m_t^2 \left(\frac{e^4 |V_{tb}|^2}{2 \sin^4 \theta_w} \right)^2 (l_1 \cdot e_1^a)(k_1 \cdot q_1)(l_2 \cdot e_2^b)(k_2 \cdot q_2) \sigma_{a(\lambda_3\lambda'_3)} \otimes \bar{\sigma}_{b(\lambda_4\lambda'_4)} \\ &\times \frac{\pi^2 \delta(p_1^2 - m_W^2) \delta(p_2^2 - m_W^2)}{(M_W \Gamma_W)^2}. \end{aligned} \quad (13)$$

With this, one can then proceed to glue together the density matrix for the production, which has been given in Ref. [4], and those for the decays of the top quarks. For the top and anti-top propagators, we shall use also the narrow width approximation. These provide another two delta functions. After that, we can write the phase space for 6 final state particles in a such way that it will be straight forward to integrate out all the delta function. The phase space can be rewritten from the standard way [3],

$$d_6(T \rightarrow k_1 l_1 q_1 k_2 l_2 q_2) = (2\pi)^4 \delta^4(T - k_1 - l_1 - q_1 - k_2 - l_2 - q_2) \frac{d^3 l_1}{(2\pi)^3 2E_{l_1}} \frac{d^3 k_1}{(2\pi)^3 2E_{k_1}} \frac{d^3 q_1}{(2\pi)^3 2E_{q_1}} \frac{d^3 l_2}{(2\pi)^3 2E_{l_2}} \frac{d^3 k_2}{(2\pi)^3 2E_{k_2}} \frac{d^3 q_2}{(2\pi)^3 2E_{q_2}} \quad (14)$$

$$\begin{aligned} &= \frac{1}{(2\pi)^4} d_2(T \rightarrow r_1 r_2) d_2(r_1 \rightarrow p_1 q_1) d_2(r_2 \rightarrow p_2 q_2) \\ &\times d_2(p_1 \rightarrow l_1 k_1) d_2(p_2 \rightarrow l_2 k_2) dr_1^2 dr_2^2 dp_1^2 dp_2^2 \end{aligned} \quad (15)$$

where $T^\mu = i_1^\mu + i_2^\mu$, with i_1 and i_2 defined as the four-momenta of the initial partons and

$$d_2(a \rightarrow bc) = (2\pi)^4 \delta^4(a - b - c) \frac{d^3b}{(2\pi)^3 2E_b} \frac{d^3c}{(2\pi)^3 2E_c} \quad (16)$$

is the phase space for a particle with four-momentum a decaying into particles with four-momenta b and c .

Combining the above results, we obtain directly the differential cross section

$$\begin{aligned} d\sigma_{ii} &= \frac{P}{4i_1 \cdot i_2} d_6(T \rightarrow k_1 l_1 q_1 k_2 l_2 q_2) \\ &= \frac{4\pi^2 \alpha_s^2}{N} \left(\frac{e^4 |V_{tb}|^2}{2 \sin^4 \theta_w} \right)^2 (k_1 \cdot q_1)(k_2 \cdot q_2) l_{1\alpha} l_{2\beta} I_{ii}^{\alpha\beta} \frac{d_2(T \rightarrow r_1 r_2)}{i_1 \cdot i_2} \\ &\quad \times \frac{d_2(r_1 \rightarrow p_1 q_1) d_2(r_2 \rightarrow p_2 q_2) d_2(p_1 \rightarrow l_1 k_1) d_2(p_2 \rightarrow l_2 k_2)}{(M_W \Gamma_W M_t \Gamma_t)^2}, \end{aligned} \quad (17)$$

N is the number of color and the indices ii designate the initial particles. We have the result for the $gg \rightarrow t\bar{t}$ case

$$\begin{aligned} I_{gg}^{\alpha\beta} &= \left(x - 1 - \frac{1}{N^2 - 1} \right) \left\{ 2r_1^\alpha r_2^\beta \left[\frac{-1}{x} + \frac{1}{\gamma^2} \left(1 - \frac{x}{2\gamma^2} \right) + 1 - \frac{x}{2\gamma^2} \right] \right. \\ &\quad - \frac{1}{2\gamma^2} \left(1 - \frac{x}{\gamma^2} \right) (r_1^\alpha T^\beta + T^\alpha r_2^\beta) + m_t^2 \left(\frac{-1}{x} + \frac{1}{\gamma^2} \left(1 - \frac{x}{2\gamma^2} \right) \right) g^{\alpha\beta} \\ &\quad \left. + \frac{1}{4\gamma^2} \left(1 - \frac{x}{2\gamma^2} \right) \left[T^\alpha T^\beta - R^\alpha R^\beta - \left(\frac{u-t}{s} \right) (R^\alpha T^\beta - T^\alpha R^\beta) \right] \right\} \end{aligned} \quad (18)$$

and for the $q\bar{q} \rightarrow t\bar{t}$ case

$$\begin{aligned} I_{q\bar{q}}^{\alpha\beta} &= \left(\frac{N^2 - 1}{2N} \right) \left\{ 2r_1^\alpha r_2^\beta \left[1 - \frac{1}{x} \left(1 - \frac{x}{2\gamma^2} \right) \right] \right. \\ &\quad - \frac{1}{2\gamma^2} (r_1^\alpha T^\beta + T^\alpha r_2^\beta) - \frac{m_t^2}{x} \left(1 - \frac{x}{2\gamma^2} \right) g^{\alpha\beta} \\ &\quad \left. + \frac{1}{4\gamma^2} \left[T^\alpha T^\beta - R^\alpha R^\beta - \left(\frac{u-t}{s} \right) (R^\alpha T^\beta - T^\alpha R^\beta) \right] \right\}. \end{aligned} \quad (19)$$

The s , t and u are the Mandelstam variable, $T^\mu = i_1^\mu + i_2^\mu$, $R^\mu = i_1^\mu - i_2^\mu$, $\gamma^2 = s/4m_t^2$ and $x = s^2/2(t - m_t^2)(u - m_t^2)$.

We want to show the spin effect of the quark. We need to compare to the case where the top quark is taken to be a spinless particle. This will allow us to pinpoint the spin effect. One way to get formula for the spinless case is to take the average of the top quark helicity

both in the production density matrix and in the decay density matrix independently before we join them together. In the usual Monte Carlo simulation for the experiments, this is indeed the approximation taken by the program. The cross section can be obtained by substituting I_{gg} and I_{qq} with

$$I_{gg}^{\alpha\beta} = \left(x - 1 - \frac{1}{N^2 - 1} \right) \left\{ r_1^\alpha r_2^\beta \left[1 - \frac{1}{x} + \frac{1}{\gamma^2} \left(1 - \frac{x}{2\gamma^2} \right) \right] \right\} \quad (20)$$

and

$$I_{qq}^{\alpha\beta} = \left(\frac{N^2 - 1}{2N} \right) \left\{ r_1^\alpha r_2^\beta \left(1 - \frac{1}{x} \left(1 - \frac{x}{2\gamma^2} \right) \right) \right\}. \quad (21)$$

For the last two equation, we should emphasize that the cross section without the spin correlation for the top quark is the one that has been used in the literature and by most of the experimental event simulators.

If one does not observe any correlation between the observables associated with the final decay products of top decays, the differential cross sections can be integrated easily in a covariant notation using well known relation for integration of two particles phase-space. One can obtain a very simple expression for the differential cross section

$$\begin{aligned} \frac{d\sigma_{ii}}{d\cos\theta} &= \frac{1}{9 \times 2^{19} \pi^3} \frac{\alpha_s^2}{N} \left(\frac{e^4 |V_{tb}|}{2 \sin^4 \theta_w} \right)^2 \left(\frac{M_W}{\Gamma_W \Gamma_t m_t} \right)^2 \left(1 - \frac{1}{\gamma^2} \right)^{1/2} \lambda(1, y_b, y_W) \\ &\times \left[1 + y_b - 2y_W + \frac{(1 - y_b)^2}{y_W} \right]^2 \frac{r_{1\alpha} r_{2\beta}}{s} I_{ii}^{\alpha\beta} \end{aligned} \quad (22)$$

where θ is the angle between the incoming parton i_1 and the top quark r_1 , $y_b = m_b^2/m_t^2$, $y_W = m_W^2/m_t^2$ and $\lambda(a, b, c) = a^2 + b^2 + c^2 - 2ab - 2ac - 2bc$. The integration over one of the top branch gives result proportional to $r_1^\alpha I_{\alpha\beta}$ or $r_2^\beta I_{\alpha\beta}$. As expected, after the integration of final phase space variables, spinless approximation gives the same result as the exact one. This can be seen as a consequence of the identities

$$r_{1\alpha} I_{gg}^{\alpha\beta} = r_{1\alpha} I_{gg}^{\alpha\beta}, \quad r_{2\beta} I_{gg}^{\alpha\beta} = r_{2\beta} I_{gg}^{\alpha\beta} \quad (23)$$

and

$$r_{1\alpha} I_{qq}^{\alpha\beta} = r_{1\alpha} I_{qq}^{\alpha\beta}, \quad r_{2\beta} I_{qq}^{\alpha\beta} = r_{2\beta} I_{qq}^{\alpha\beta}. \quad (24)$$

The result not only confirms that the interference effects indeed vanish when integrated over the complete phase space, but also, that if one integrates over all the phase space variables associated to the decay products of just *one* of the top quarks, the spin interference effect will disappear. Equivalently if we measure any observables related to only one of the top(or anti-top) quark, the effect will not show up. Therefore, to measure interference effect, we need to find observables that correlate the kinematic variables associated with the particles from the top quark decay and those from the anti-top quark decay. Intuitively, it is not obvious what is the best correlated observable which can probe this interference effect. For the rest of this paper, we shall present our attempts in this direction.

Before we discuss how to probe the interference effect, one should note that Eq.(22) can be further simplified. The widths can be replaced by branching ratios using $\Gamma_t = \Gamma_{t \rightarrow Wb}/Br(t \rightarrow Wb)$ and $\Gamma_W = \Gamma_{W \rightarrow \bar{l}\nu_l}/Br(W \rightarrow \bar{l}\nu_l)$. The partial widths can be calculated trivially at tree level, and the branching ratios can be evaluated by summing over all the possible channels for top desintegration. The $\cos\theta$ integration can also be performed to reproduce the well-known result [3]

$$\sigma_{qq} = \frac{4\pi\alpha_s^2}{9s}\beta \left(1 - \frac{\beta^2}{3}\right) \quad (25)$$

and

$$\sigma_{gg} = \frac{\pi\alpha_s^2}{48s}\beta \left[(66 - 36\beta^2 + 2\beta^4) \frac{1}{2\beta} \ln\left(\frac{1+\beta}{1-\beta}\right) - 59 + 31\beta^2 \right] \quad (26)$$

where $\beta^2 = 1 - 1/\gamma^2$.

To probe the interference effect, we shall look for observables related to the final decay products, instead of using directly the top momenta which need to be reconstructed. The easiest observables to try are those related to the two charged leptons (electron or muon) from the leptonic decays of two W 's. The advantage is that these particles can be easily observed in a hadron collider. On the other hand, the dilepton decays has lower branching ratios, which reduces the statistics. For this case, we have investigated the effect of interference on the distribution of (1) their total energy $E_{l_1} + E_{l_2}$, (2) their total z-momentum $l_{1z} + l_{2z}$, (3)

an orthogonal combination $l_{1z} - l_{2z}$, (4) the cosine of the angle between these two charged leptons and (5) the asymmetries A_p and A_\perp to be defined later. To get these distributions as a function of the observables, the numerical integration program (VEGAS) is used. The top quark mass is taken to be $m_t = 176$ GeV in all numerical analyses.

In Fig. 1, we show the differential cross section $d\sigma/dv_1$ for the quark-antiquark collision where $v_1 = (E_{l_1} + E_{l_2})/\sqrt{s}$. We show curves a, b, c, d and e for $\sqrt{s} = 400, 500, 700, 1000$ and 2000 GeV. At each energy, we plot the cross section with (without) interference effect with solid (dash) lines. We found that, for the quark-antiquark collision, in the central (peak) region the interference effect decreases the cross section while at the two shoulders, it enhances the cross section. In addition, while the overall cross section decreases roughly as $1/s$ as s increases, the percentage decrease of the maximum value of $d\sigma/dv_1$ due to the interference effect actually increases as s . (For example, for $\sqrt{s} = 400$ GeV, the peak of the cross section decreases from 1.17 pb to 1.15 pb, while, for $\sqrt{s} = 1$ TeV, it decreases from .19 pb to .17 pb.) In other words, comparing to the spinless case, the effect of the interference gets stronger as the total energy increases.

In Fig. 2.I and 2.II, we show the same differential cross section $d\sigma/dv_1$ for the gluon fusion case. Again, we plot the cross section with (without) interference effect using solid (dash) lines. In Fig. 2.I, we use $\sqrt{s} = 400, 500$ GeV for curves a, b and, in Fig. 2.II, we use $\sqrt{s} = 700, 1000$ and 2000 GeV for curves c, d and e respectively. For $\sqrt{s} < 700$ GeV, unlike the previous case, the cross section increases with s as is well-known. And here, also in stark contrast with the previous case, the effect of the interference increases the values of the cross section in the region near the peak, while making the values at the two shoulders decrease. However, for higher total energy \sqrt{s} , the behavior become the same as the case for $q\bar{q}$. One should also note that the interference effects for gluon fusion case appear to be always smaller than that for the quark-antiquark production process.

In Fig. 3 and Fig. 4, we show distribution of $d\sigma/dv_2$ as a function of $v_2 = (l_1^z + l_2^z)/\sqrt{s}$ for quark-antiquark ($q\bar{q}$) production and for gluon fusion (gg) production respectively. The l_1^z is the z -component of the momentum, l_1 , of the lepton from top decay where the z is

defined to be the direction of parton i_1 which is also the beam axis. Similarly, one defines l_2^z with the same definition of z -axis. The curves a, b, c and d in Fig. 3 for $q\bar{q}$ case correspond to $\sqrt{s} = 400, 500, 700$ and 1000 GeV while, in Fig. 4 for gg case, the curves a, b and c correspond to $\sqrt{s} = 400, 450$ and 500 GeV. In $q\bar{q}$ case, the interference effect always increases the peak of the distribution. In addition, the percentage increase of the effect decreases with \sqrt{s} but only mildly. For gluon fusion case, below $\sqrt{s} = 700$ GeV, the peak of the distribution is reduced by the interference effect and then become larger for \sqrt{s} over 1 TeV. However, the effect is smaller than the $q\bar{q}$ case in general.

We have also analyzed the effect of the interference on the distribution of $d\sigma/dv_3$ as a function of $v_3 = (l_1^z - l_2^z)/\sqrt{s}$. We found the interference effect to be negligibly small at \sqrt{s} below 700 GeV for $q\bar{q}$ production. The effect is even smaller for all the other \sqrt{s} and for the case of gg production.

A potentially very interesting way to observe the interference effect is to measure the distribution of angle between the two final leptons. We get a good signal of the interference effect near the threshold of the $t\bar{t}$ production. For $q\bar{q}$ production, we plot in Fig. 5.II, the differential cross section $d\sigma/d\cos\theta_{ll}$ as a function of $\cos\theta_{ll}$. The curves a, b and c correspond to $\sqrt{s} = 400, 500$ and 700 GeV and θ_{ll} is the angle between the two lepton. For comparison, we plot in Fig. 5.I, the differential cross section $d\sigma/d\cos\theta_{WW}$ as a function of $\cos\theta_{WW}$ for the same \sqrt{s} , where θ_{WW} is the angle between the two W bosons. Somewhat unexpectedly, we found that the signal of interference is much stronger in $d\sigma/d\cos\theta_{ll}$ than that in the case of $d\sigma/d\cos\theta_{WW}$. This difference seems to indicate that at the level of W^+W^- in addition to the asymmetry carried by the the kinematic variable $\cos\theta_{WW}$, some asymmetry due to the interference is carried by the helicity information of the W bosons. This helicity-related asymmetry is turned into the leptonic angular asymmetry as W bosons decay. As a result, the angular asymmetry for the angle between the leptons provides more sensitive signal than the angular asymmetry for the angle between the W bosons. We can see that both side of the distribution for leptons case change by more than 25 % . For increasing \sqrt{s} up to 1 TeV, the $q\bar{q}$ collision still show a large difference between the cross sections with and without the

interference effect.

For the gluon fusion, we also produce the distributions $d\sigma/d\cos\theta_{WW}$ and $d\sigma/d\cos\theta_{ll}$, as shown in Fig. 6.I and Fig. 6.II. The curves a, b and c correspond to $\sqrt{s} = 400, 450$ and 500 GeV. At $\sqrt{s} = 400$, the two distributions for $d\sigma/d\cos\theta_{ll}$ differ dramatically from each other up to a factor 2. However, the difference is reduced quickly as \sqrt{s} increases, the difference is negligible at $\sqrt{s} = 700$ GeV. The most important characteristic is that, in contrast with Fig. 1–4, the signal does not just consist of a change in the width or height, but a change in the shape of whole distribution and therefore may provide an easier signature for experiments.

The other interesting observables are the following two new kinds of asymmetries. In these asymmetries, one looks at the directions of momenta of two particles and compares if they are on the same side of a defining plane or on the opposite side. The asymmetry can be defined as $A = (N_{\text{same}} - N_{\text{opposite}})/(N_{\text{same}} + N_{\text{opposite}})$. For the first asymmetry, the plane is the production plane defined by the beam axis and the direction of the top quark. The two incoming partons and the two top quarks lie on this plane. The asymmetry associated with this plane will be called A_p . For the second asymmetry, the defining plane is to be the one that is perpendicular to the beam axis. The associated asymmetry will be called A_{\perp} .

In Fig. 7a, we show A_p as a function of \sqrt{s} using the momenta of the two final leptons to define asymmetry. As a comparison, in Fig. 7b, we show the same asymmetry but now using the momenta of the two W bosons as the defining directions. The solid lines are for the case of $q\bar{q}$ production. The dotted lines are for gluon fusion. The asymmetry should vanish without the interference effect. Note that just as the earlier cases, the asymmetry is more pronounced when measured by the final leptons, instead of by the intermediate, polarized W bosons. As shown in Fig. 7a, the asymmetry, A_p , can be as large as 5-10 percent. Experimentally it is also important to note that this asymmetry is invariant under a boost in the beam direction. Therefore, as long as the transverse momenta of the initial partons are small, the asymmetry is more or less insensitive to the longitudinal momenta of the initial partons.

In Fig. 8, we show A_{\perp} as a function of \sqrt{s} . Here we present only the result for the case

in which the momenta of the two final leptons are used to define asymmetry. Just as the previous case, if the W momenta are used instead of the lepton momenta, the asymmetry is smaller. The solid line is for $q\bar{q}$ production including the interference effect. The dash line is for $q\bar{q}$ production without the interference effect. The dotted line is for gg fusion including the interference effect. The dash-dot line is for gg fusion without the interference effect. As shown in the figure, the asymmetries in all these channels are all negative with sizes of order .4-.7. Unfortunately, this asymmetry is sensitive to whether the initial partons are colliding in their center of mass in the Lab. frame or not. Therefore, it is probably harder to isolate the effect from the background.

In conclusion, we have obtained an analytic formula for the cross section of the top quark pair production and their decays into b quarks and W bosons which, in turns, decay into two fermions. Our result includes the interference effect due to the fact that top quarks carry spin and therefore the intermediate states have more than one spin channels. A measurement of this interference effect can be seen as the direct measurement of the spin effect of the top quarks. To demonstrate the use of these analytic results, we use them to search for observables that may provide a good measurement of the interference effect. While none of the observables may be straightforward to measure, we show that appreciable effects might be observable in the asymmetries defined by the relative angular distributions of the leptons coming from both W bosons. More realistic simulation needs to be carried out before these potential observables can prove to be useful experimentally.

ACKNOWLEDGMENTS

We would like to thank Alexei Sumarokov for useful discussions. This work is supported by the National Science Council of Republic of China under grants NSC84-2811-M008-001(for S.L), NSC84-2112-M007-042, NSC84-2112-M007-016(for D.C. and P.T.).

REFERENCES

- [1] F. Abe *et al.* Phys. Rev. Lett. **73**, 225, 1994; F. Abe *et al.* Phys. Rev. D**50**, 2966, 1994.
- [2] I. Bigi and H. Krasemann, Z. Phys. **C7** 127 (1981); I. Bigi, Y. Dokshitzer, V. Khoze, J. Kuhn and P. Zerwas, Phys. Lett. B **181** 157 (1986).
- [3] V. Barger and R. J. N. Phillips, *Collider Physics*, Addison-Wesley (1987), Appendix B.
Note that our convention for d_n is different from the one used in the book by $(2\pi)^{4-3n}$.
- [4] S.C. Lee, Phys. Lett. B **189**, 461, 1987.
- [5] G.P. Lepage, Cornell University preprint CLNS-80/447 1980; J. Comp. Phys. 27, 192, 1978.
- [6] K. Hagiwara, D. Zeppenfeld, Nucl. Phys. B **274**, 1, 1986.
- [7] G.L. Kane, G.A. Ladinsky, C.-P. Yuan, Phys. Rev. D **45**, 124, 1992.
- [8] C. Bouchiat, L. Michel. Nucl. Phys. 5, 416, 1958; L. Michel Suppl. Nuovo Cim. **14** (1959) 95.

FIGURES

Fig. 1. The differential cross section $d\sigma/dv_1$ with (without) interference effect using solid (dash) lines for the quark-antiquark collision. The curves a, b, c, d and e correspond to $\sqrt{s} = 400, 500, 700, 1000$ and 2000 GeV.

Fig. 2. Same as Fig. 1 but for the gluon fusion.

Fig. 3. The differential cross section $d\sigma/dv_2$ with (without) interference effect using solid (dash) lines for the quark-antiquark collision. The curves a, b, c and d correspond to $\sqrt{s} = 400, 500, 700$ and 1000 GeV.

Fig. 4. The differential cross section $d\sigma/dv_2$ with (without) interference effect using solid (dash) lines for the gluon fusion. The curves a, b and c correspond to $\sqrt{s} = 400, 450$ and 500 GeV.

Fig. 5. The differential cross section (I) $d\sigma/d \cos \theta_{WW}$ and (II) $d\sigma/d \cos \theta_l$ with (without) interference effect using solid (dash) lines for the quark-antiquark collision. The curves a, b and c correspond to $\sqrt{s} = 400, 500$ and 700 GeV.

Fig. 6. The differential cross section (I) $d\sigma/d \cos \theta_{WW}$ and (II) $d\sigma/d \cos \theta_l$ with (without) interference effect using solid (dash) lines for the gluon fusion. The curves a, b and c correspond to $\sqrt{s} = 400, 450$ and 500 GeV.

Fig. 7. The asymmetry A_p using (a) the two final leptons and (b) the momenta of the two W bosons to define directions. The solid (dash) lines correspond to the case of $q\bar{q}$ production (gluon fusion).

Fig. 8. The asymmetry A_\perp as a function of \sqrt{s} . The solid (dash) line is for $q\bar{q}$ production including (without) the interference effect. The dotted (dash-dot) line is for gg fusion including (without) the interference effect.

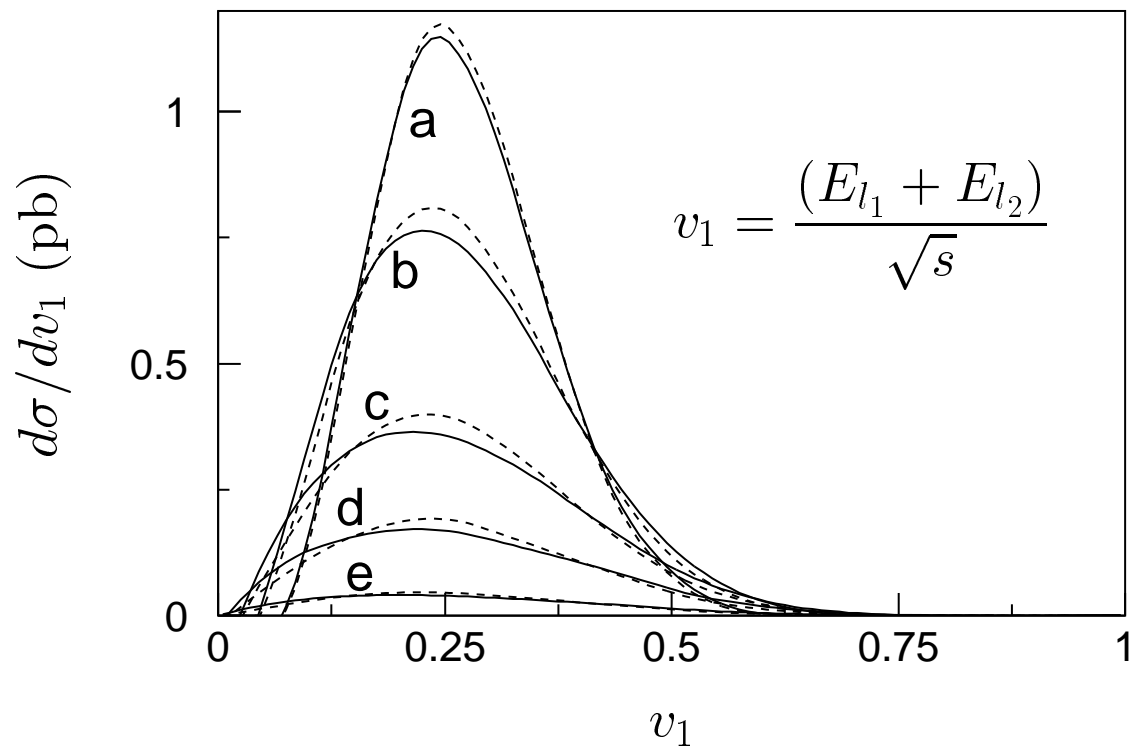


FIG. 1

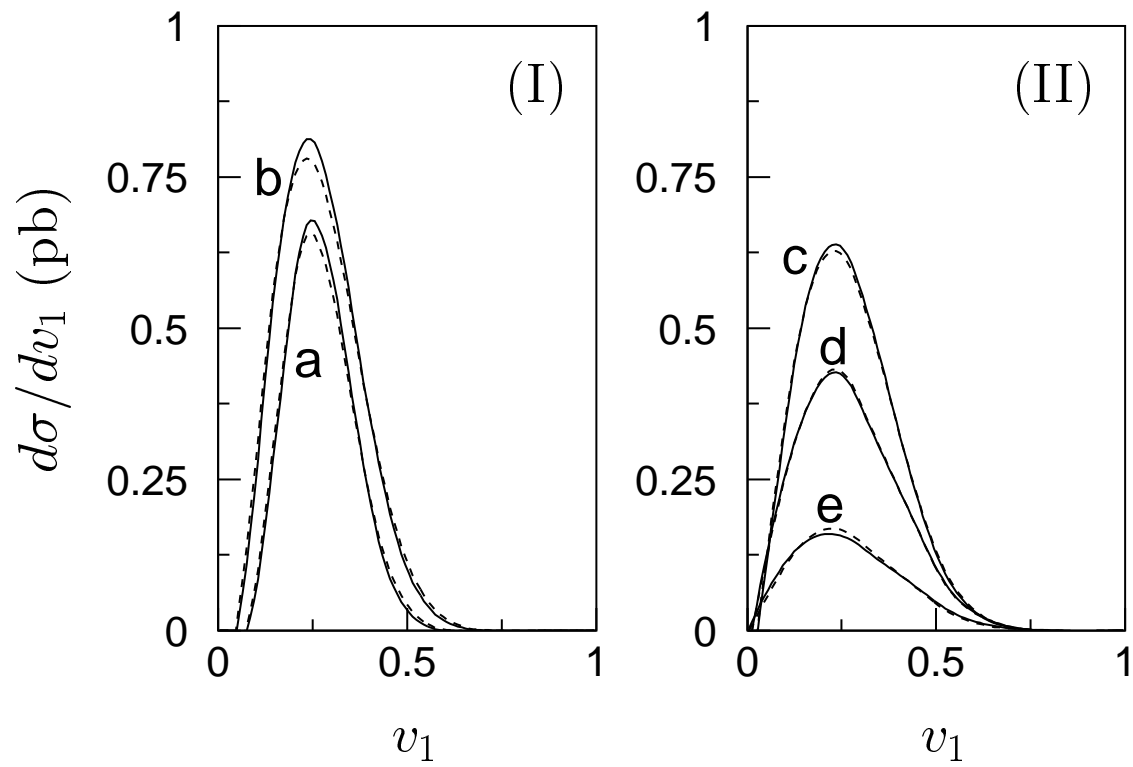


FIG. 2

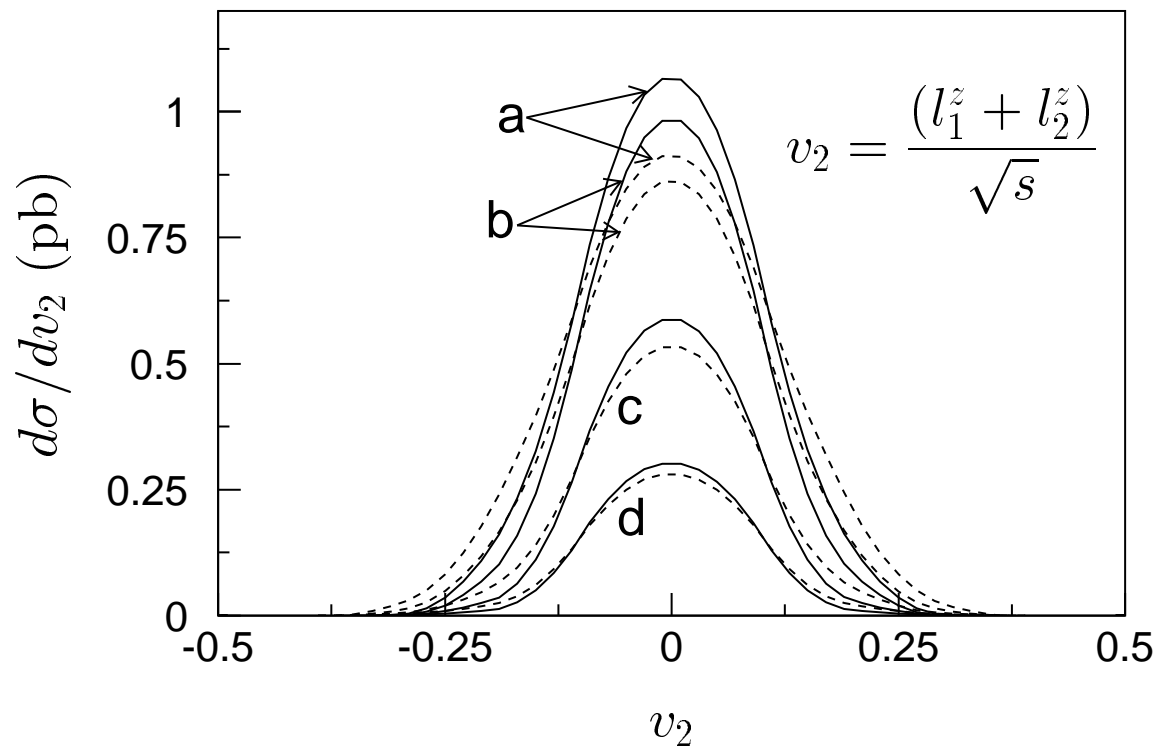


FIG. 3

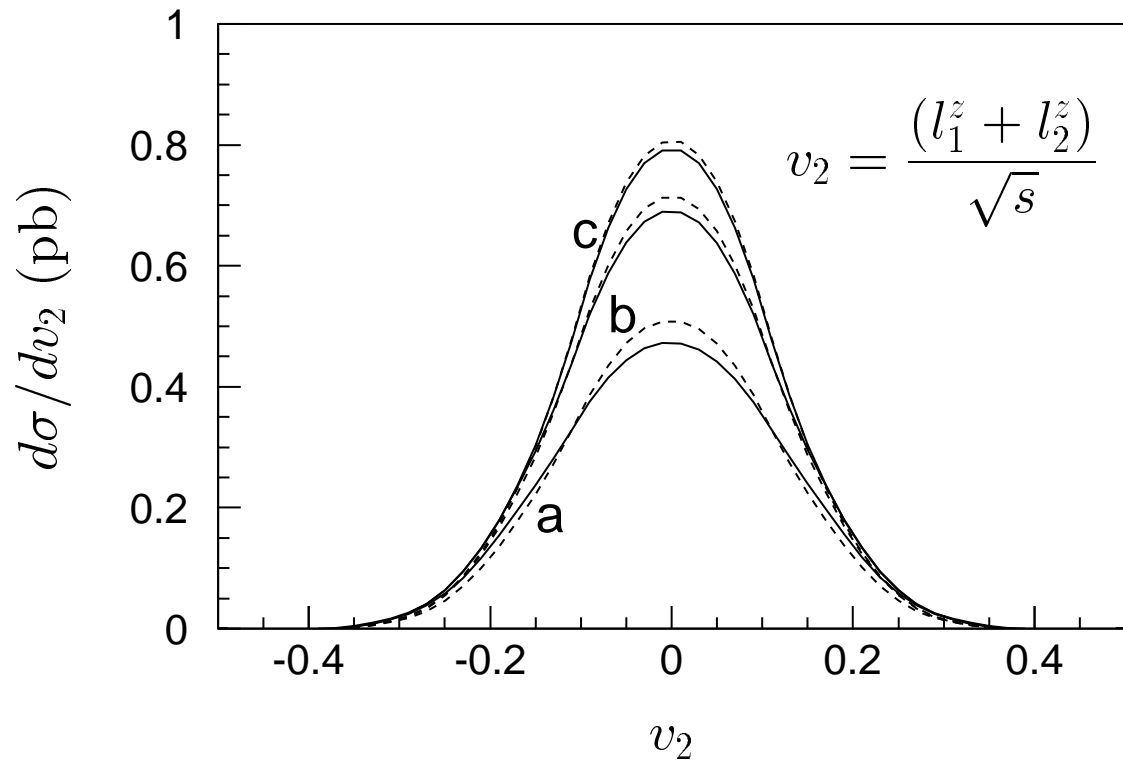


FIG. 4

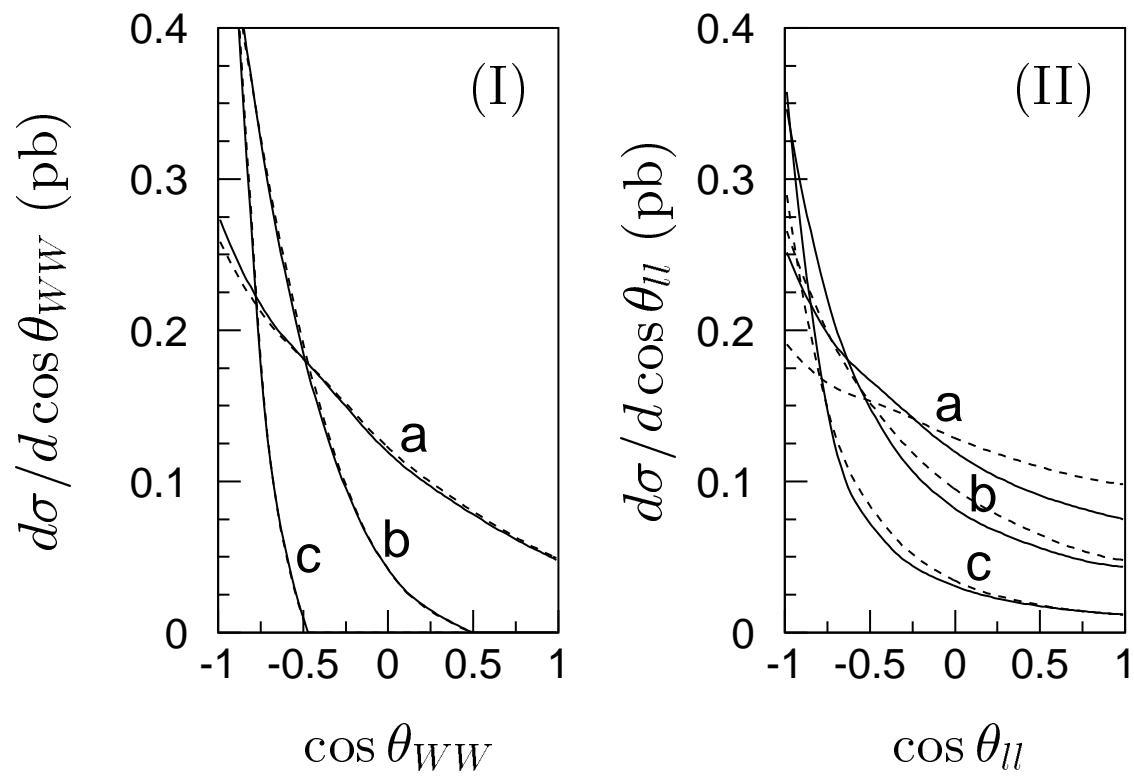


FIG. 5

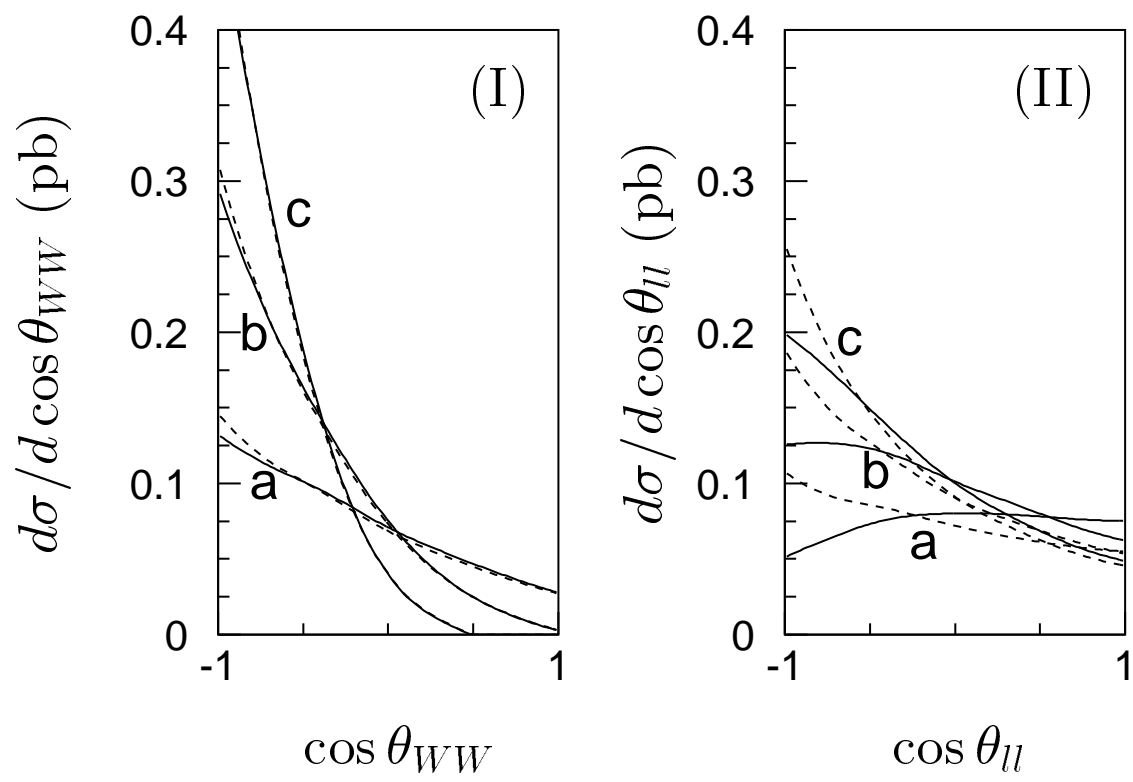


FIG. 6

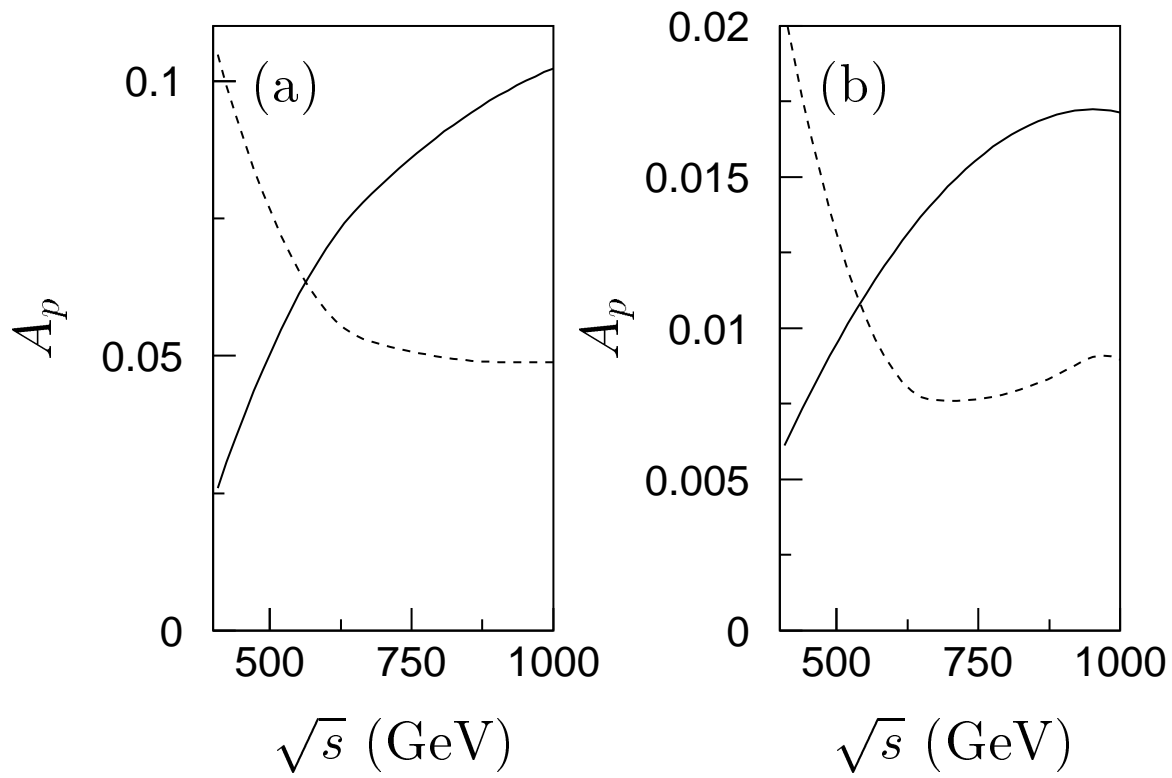


FIG. 7

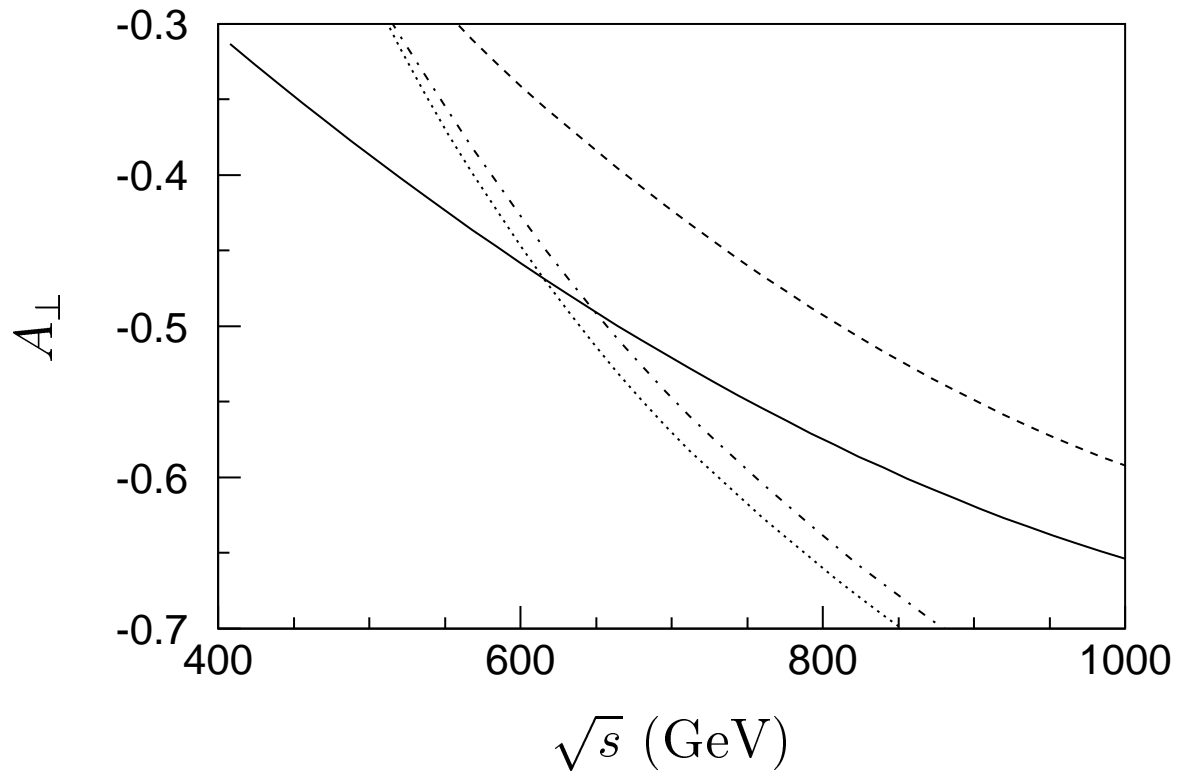


FIG. 8